Journal of Materials Chemistry C

PAPER

View Article Online
View Journal

Cite this: DOI: 10.1039/c9tc02773d

Novel blue fluorescent emitters structured by linking triphenylamine and anthracene derivatives for organic light-emitting devices with EQE exceeding 5%†

Jing Zhang,[a] Yaping Zhao,[a] Huixia Xu,*[a] Di Zhang,[a] Yanqin Miao,*[a] Ruth Shinar,[b] Joseph Shinar,[c] Hua Wang,[a] Bingshe Xu[a] and Yucheng Wu[a]

Received 24th May 2019,
Accepted 5th August 2019

DOI: 10.1039/c9tc02773d

rsc.li/materials-c

Achieving an external quantum efficiency exceeding 5% for traditional blue fluorescent organic light emitting devices (OLEDs) is still a current challenge due to the 25% limit of the radiative exciton yield. Bipolar organic molecules with a special hybrid local-excited and charge-transfer state have showed huge potential to address this issue. Herein, we designed and synthesized two novel bipolar compounds, namely **TPA-AN-NA** and **TPA-AN-TFP**, which were structured by simply linking a donor of triphenylamine (TPA) and both acceptors of anthracene derivatives. Both resulting compounds show good blue emission with emission peaks at 468 and 471 nm and photoluminescence quantum yields of 30.68 and 23.96% in thin films for **TPA-AN-NA** and **TPA-AN-TFP**, respectively. They also exhibit good solubility and can dissolve in several organic solvents with different polarities. Further, the fabricated blue OLEDs with **TPA-AN-NA** and **TPA-AN-TFP** as emitters also realize the corresponding blue emission well with electroluminescence peaks at 464 and 472 nm, respectively. The **TPA-AN-NA**-based blue device achieves a high external quantum efficiency of 5.44% and a radiative exciton yield of 56.68%, exceeding the theoretical limit.

Introduction

Organic light-emitting devices (OLEDs) are widely considered to be the next generation display and potential lighting technologies due to their unique attributes of high colour contrast, efficiency, light weight, and special flexibility.[1–3] Emitting materials are the prerequisites for developing high performance OLEDs. Numerous efforts have been made for obtaining high performance emitting materials with high quantum yield, good colour purity, and long-term stability. However, compared with the long-band emitting materials (green and red), the blue ones are still very rare due to their intrinsic large energy gap, poor thermal stability, and low photoluminescence quantum yield (Φ_{PL}),[4–7] which becomes a bottleneck for the development of OLEDs. Typically, in traditional blue fluorescent OLEDs, only 25% single excitons can emit radiatively, while 75% triplet excitons decay non-radiatively.[8,9] The external quantum efficiency (EQE) of fluorescent OLEDs is limited to only 5%, which is not beneficial for developing high efficiency OLEDs.[10–12] Therefore, an effective way to boost the device efficiency of blue OLEDs is to enable the contribution of non-emissive triplet excitons to light emission, consequently, breaking the 25% limitation of the radiative exciton yield (η_r).

Donor–acceptor (D–A)-type bipolar organic molecules with special excited states have displayed tremendous potential to address the above-mentioned issue.[13,14] Generally, the charge-transfer (CT) excited state in D–A molecules with the weak bonding energy of the exciton facilitates efficient reverse intersystem-crossing (RISC) from triplet to singlet to improve η_r.[15–17] Simultaneously, the locally excited (LE) state with a high oscillator strength can enhance Φ_{PL} owing to the overlap of the highest occupied molecular orbital (HOMO) and the lowest unoccupied molecular orbital (LUMO).[18] This unique hybrid local and charge transfer (HLCT) excited state in D–A molecules can simultaneously contribute to high η_r and high Φ_{PL}, consequently improving the electroluminescence efficiency of blue fluorescent OLEDs.[19–21]

In order to construct efficient blue-light emitting materials with the HLCT state, the donor and acceptor units should be carefully selected to regulate the LE and CT excited states. Additionally, to avoid the long-band emission, neither a strong

[a] Key Laboratory of Interface Science and Engineering in Advanced Materials, Ministry of Education, Taiyuan University of Technology, Taiyuan 030024, China. E-mail: xuhuixia@tyut.edu.cn, miaoyanqin@tyut.edu.cn
[b] Microelectronics Research Canter and Electrical & Computer Engineering Department, Iowa State University, Ames, IA 50011, USA
[c] Ames Laboratory, USDOE and Physics & Astronomy Department, Iowa State University, Ames, IA, 50011, USA

† Electronic supplementary information (ESI) available. See DOI: 10.1039/c9tc02773d

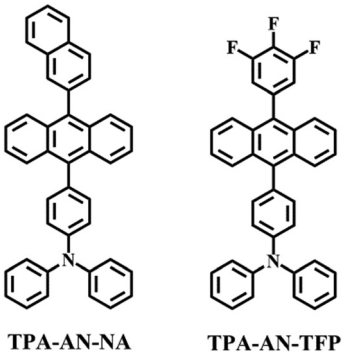

Fig. 1 Molecular structures of **TPA-AN-NA** and **TPA-AN-TFP**.

donor nor acceptor should be chosen.[10] Triphenylamine (TPA) is a medium electron-donating group with a unique space propeller structure with large steric hindrance, which can effectively reduce the exciton binding energy and favour the formation of the CT state.[22–24] Anthracene (An) is a weak electron-withdrawing group with a planar conjugated structure, which will promote the overlap between the HOMO and LUMO and improve the LE state.[25–29]

Herein, two novel bipolar compounds were synthesized by simply linking a donor of TPA and both acceptors of anthracene derivatives, namely **TPA-AN-NA** and **TPA-AN-TFP**, respectively. The molecular structures of the two blue emitters are shown in Fig. 1. As expected, two resulting compounds show good blue emission with emission peaks at 468 and 471 nm and photoluminescence quantum yields of 30.68 and 23.96% for **TPA-AN-NA** and **TPA-AN-TFP** in thin films, respectively. And the fabricated OLED with **TPA-AN-NA** and **TPA-AN-TFP** as emitters also realize the corresponding blue emission well with the EL peak at 464 and 472 nm, respectively. Moreover, the **TPA-AN-NA**-based blue device shows excellent electroluminescence performance with a maximum current efficiency (CE), power efficiency (PE), and external quantum efficiency (EQE) reaching 7.16 cd A^{-1}, 6.09 lm W^{-1}, and 5.44%, respectively, where the EQE is obviously higher than the reported limit of 5%. These results demonstrate that the TPA-and An-based emitters have promising application in blue OLEDs.

Results and discussion

Structure characteristics

The synthetic routes and molecular structures of **TPA-AN-NA** and **TPA-AN-TFP** are depicted in Scheme S1 (ESI†) and Fig. 1. The intermediate compound **1** and the two target products were prepared through the palladium catalysed Suzuki coupling reaction, and then purified by column chromatography on silica gel. The chemical structures of the compounds were confirmed by ^{1}H NMR and ^{13}C NMR, as shown in the ESI.† There are large torsion angles of 68° between TPA and the adjacent phenyl ring and 72° between anthracene and the phenyl ring in compound **TPA-AN-NA** (Fig. 2). When electron-withdrawing 3,4,5-trifluorophenyl is introduced into compound **TPA-AN-TFP**, the two torsion angles are increased to

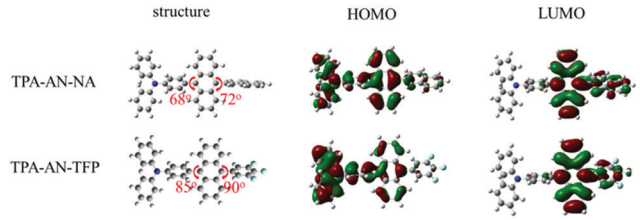

Fig. 2 Optimized structure and spatial distribution of the HOMO and LUMO orbitals of **TPA-AN-NA** and **TPA-AN-TFP**.

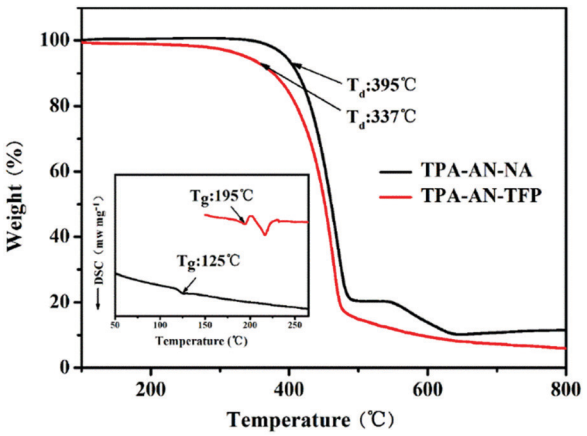

Fig. 3 TGA and DSC (inset) curves of **TPA-AN-NA** and **TPA-AN-TFP**.

85 and 90°, respectively. The conjugation effect between anthracene and trifluorophenyl was completely suppressed. The comparison showed that both the compounds exhibited similar LUMO distributions, which are mainly located in the anthracene moieties (Fig. 2). The HOMO of **TPA-AN-NA** was mostly populated on anthracene and extended to the TPA unit, with a little contribution from naphthalene, while the HOMO of **TPA-AN-TFP** was largely contributed to the TPA group and anthracene.

The thermal stabilities were investigated by TGA and DSC under a nitrogen atmosphere. As presented in Fig. 3 and Table 1, compounds **TPA-AN-NA** and **TPA-AN-TFP** exhibit high decomposition temperatures (T_d, corresponding to 5% weight loss) of 395 and 337 °C, respectively, and high T_gs of 125 and 195 °C due to the rigid structure of the anthracene unit. These results suggest that the two compounds exhibit good thermal and morphological stabilities, which are important for applications in organic electronic devices.

Photophysical properties

The UV-vis absorption and emission spectra in CH_2Cl_2 solution and the neat film of **TPA-AN-NA** and **TPA-AN-TFP** at room temperature are shown in Fig. 4. The relevant data are also summarized in Table 1. The absorption peaks below 300 nm are attributed to the π–π* transitions of benzene rings, while the longer wavelength band absorptions appear in the range of 300–400 nm, characteristic of the π–π* transitions from anthracene and TPA. The absorption spectra of **TPA-AN-NA** and **TPA-AN-TFP** displayed similar patterns, suggesting that

Table 1 The photophysical, electrochemical and thermal properties of **TPA-AN-NA** and **TPA-AN-TFP**

Compound	λ_{abs} [a] (nm)	λ_{em} [a] (nm)	λ_{abs} [b] (nm)	λ_{em} [b] (nm)	E_g [c] (eV)	HOMO/LUMO (eV)	Φ_{PL} [d] (%)	T_d/T_g [e] (°C)
TPA-AN-NA	360, 378, 398	495	362, 383, 402	468	2.86	−5.37/−2.51	30.68	395/125
TPA-AN-TFP	355, 375, 395	506	360, 379, 400	471	2.83	−5.41/−2.58	23.96	337/195

[a] Measured in CH_2Cl_2 solution. [b] Measured in the neat film. [c] Obtained from the intersection of absorption and emission spectra. [d] Quantum yield (Φ_{PL}) from the pure film. [e] From TGA and DSC measurements.

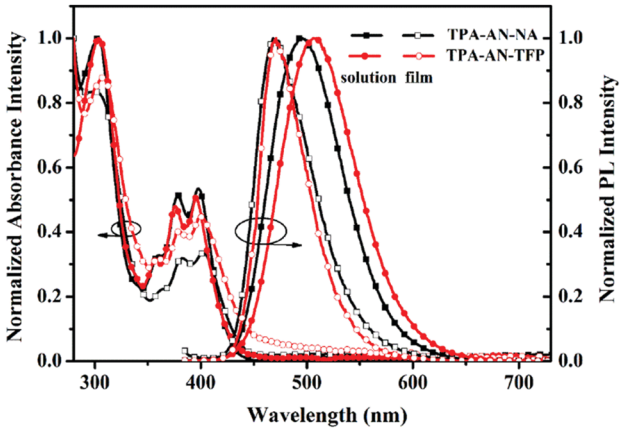

Fig. 4 The UV-vis absorption and emission spectra in CH_2Cl_2 solution and the neat film at room temperature of **TPA-AN-NA** and **TPA-AN-TFP**.

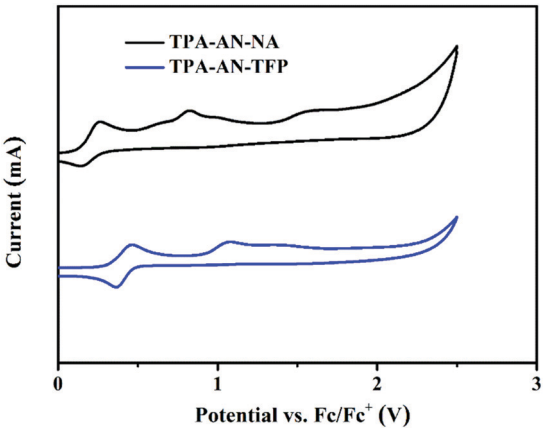

Fig. 5 Cyclic voltammograms of **TPA-AN-NA** and **TPA-AN-TFP** in CH_2Cl_2 solution.

the electron-withdrawing 3,4,5-trifluorophenyl has no effect on the ground state.

The maximum emission peaks of **TPA-AN-NA** and **TPA-AN-TFP** in CH_2Cl_2 solution were observed at 495 and 506 nm, respectively. Compared with **TPA-AN-NA**, the emission of **TPA-AN-TFP** displayed a redshift of 11 nm due to the introduction of the electron-withdrawing F atoms. It is noteworthy that the emission peaks of **TPA-AN-NA** and **TPA-AN-TFP** in films exhibit large blue-shifts of ~27 and ~35 nm relative to those in CH_2Cl_2 solution, located at 468 nm and 471 nm, respectively, which is attributed to the large dihedral angle between anthracene and TPA.

The optical band-gaps (E_g) of **TPA-AN-NA** and **TPA-AN-TFP** were calculated to be 2.86 and 2.83 eV, respectively, from the intersection between the absorption and emission spectra in films. The cyclic voltammograms (CV) of **TPA-AN-NA** and **TPA-AN-TFP** are presented in Fig. 5. The HOMO level (E_{HOMO}) was calculated according to eqn (1)

$$E_{HOMO} = -4.8 - e(E_c^{ox} - E_f^{ox})V \quad (1)$$

where E_c^{ox} is the first oxidation peak measured from the CV curve and E_f^{ox} is the oxidation peak of ferrocene. The LUMO level (E_{LUMO}) was calculated from eqn (2)

$$E_{LUMO} = E_{HOMO} + E_g \quad (2)$$

Both **TPA-AN-NA** and **TPA-AN-TFP** have almost the same HOMO levels (−5.37 and −5.41 eV) due to the same donor of TPA. A LUMO level of −2.58 eV for compound **TPA-AN-TFP** is lower than that of −2.51 eV for **TPA-AN-NA** because of the electron-withdrawing ability of 3,4,5-trifluorophenyl.

Solvatochromic effect

To understand the nature of the excited states, the absorption (Fig. S3, ESI†) and emission (Fig. 6) spectra of **TPA-AN-NA** and **TPA-AN-TFP** were examined in different solvents. The absorption spectra were insensitive to the solvent polarity, suggesting the low dipole potential in the ground state. Unlike the absorption spectra, the emission of **TPA-AN-NA** and **TPA-AN-TFP** showed an obvious solvatochromic effect. As the solvent polarity increased from the low-polarity hexane to the high-polarity dimethyl sulfoxide (DMSO), the emission peaks of **TPA-AN-NA** and **TPA-AN-TFP** exhibited red-shifts of 92 and 104 nm, respectively, which correspond to the remarkable CT-state characteristics. The emission of **TPA-AN-TFP** demonstrates a relatively large red-shift due to the strong CT-state character from TPA to trifluorophenyl and anthracene. The Lippert–Mataga model was applied for the estimation of the excited state dipole moments with the increase of solvent polarity.[30] The two compounds exhibited two section linear relations ($0.0012 \leq f \leq 0.1$ and $0.2 \leq f \leq 0.305$), as shown in Fig. S4 (ESI†), corresponding to the LE state with a small slope in low-polarity solvents ($0.0012 \leq f \leq 0.1$) and the CT state with a large slope in high-polarity solvents ($0.2 \leq f \leq 0.305$). In moderate-polarity solvents ($0.1 \leq f \leq 0.2$), such as chloroform and ethyl ether, they may possess a hybridized local and charge transfer (HLCT) state. The excited dipole moment (μ_e) values of **TPA-AN-NA** and **TPA-AN-TFP** were estimated to be 3.73 and 7.63 D in low-polarity solvents and increased to 21.72 and 24.72 D in high-polarity solvents, respectively. Therefore, they possess the LE excited state ($\mu_e < 10$ D) in low-polarity solvents and the dominant-CT state ($\mu_e > 20$ D) in high-polarity solvents according to HLCT theory.[31]

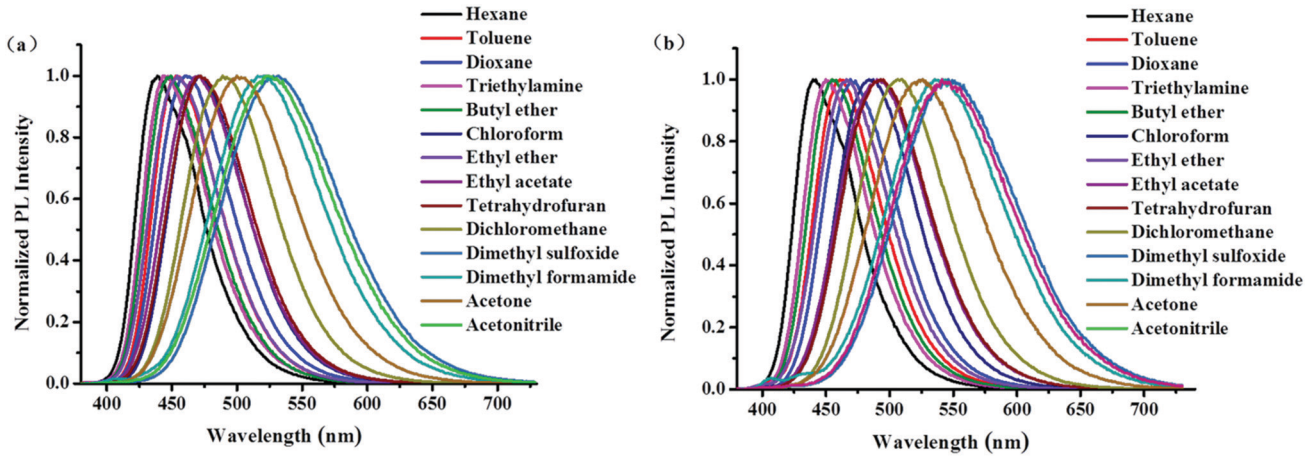

Fig. 6 The emission spectra of **TPA-AN-NA** (a) and **TPA-AN-TFP** (b) in different solvents.

The transient decay curves in different solvents and thin films were measured (Fig. S5 and S6; Tables S1 and S2, ESI†). With increasing polarities, the lifetimes increased with single exponential, indicating that there was a change from the LE to CT state. The transient PL spectra in moderate-polarity solvents (ethyl ether and tetradydrofunan) can be well fitted to a single exponential decay as shown in Tables S1 and S2 (ESI†), revealing the HLCT feature of the excited state.[32]

To further verify the HLCT characteristics of both compounds, the excited states were calculated by TD-DFT. For **TPA-AN-NA**, the hole and particle of S_1 showed spatial separation and partly orbital overlap (Fig. S7, ESI†). The separation section facilitated the CT state, and the certain orbital overlap led to the LE state, indicating the formation of HLCT components. On the other hand, the S_1 of **TPA-AN-TFP** displayed CT due to the completely separate hole and particle. The low-lying triplet state T_1 of the two materials was the LE state because their hole and particle were almost completely overlapped. The high-lying T_3 of **TPA-AN-NA** and T_2 of **TPA-AN-TFP** possess the obvious HLCT states. The energy gaps of the S_1 and T_1 of **TPA-AN-NA** and **TPA-AN-TFP** reached 1.22 and 1.10 eV, and therefore, the RISC process from the T_1 to S_1 state by TADF was prevented (Fig. 7). For **TPA-AN-NA**, the singlet–triplet energy splitting between S_1 and T_3 states of 0.004 eV enables a more competitive RISC from T_3 to S_1. A similar process occurred between S_1 and T_2 of **TPA-AN-TFP** due to the small energy gap of 0.02 eV. Therefore, the RISC of the two compounds can be achieved by a "hot exciton" process, due to which the triplet exciton originated from the high-lying states T_3 and T_2, respectively.

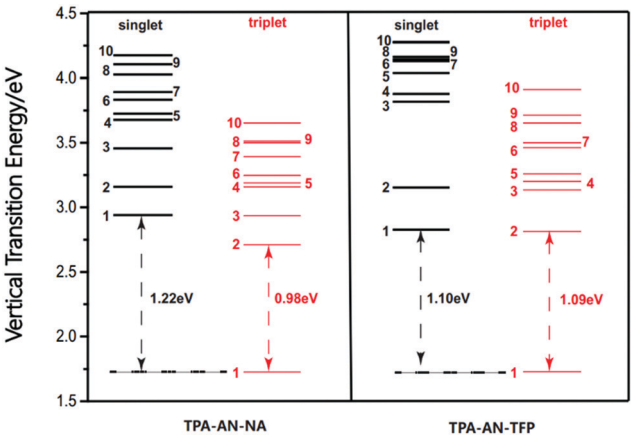

Fig. 7 Excited state (singlet and triplet) energy diagrams of **TPA-AN-NA** and **TPA-AN-TFP**.

Electroluminescence performance

The above characterization analysis indicates that **TPA-AN-NA** and **TPA-AN-TFP** as blue emitters have the potential for the development of high-performance blue OLEDs. In order to evaluate the EL characteristics of **TPA-AN-NA** and **TPA-AN-TFP**, firstly, non-doped devices with **TPA-AN-NA** and **TPA-AN-TFP** as emitters were fabricated, and the device structure was as follow: ITO/MoO_3 (3 nm)/NPB (30 nm)/TCTA (10 nm)/**TPA-AN-NA** or **TPA-AN-TFP** (20 nm)/TPBi (50 nm)/LiF (1 nm)/Al (100 nm). In these devices, ITO and Al were used as the anode and the cathode, respectively; MoO_3 and LiF acted as the hole and electron injection layers, respectively; *N*,*N*′-di(1-naphthyl)-*N*,*N*′-diphenyl-(1,1′-biphenyl)-4,4′-diamine (NPB) and tris(4-carbazoyl-9-ylphenyl)amine (TCTA) served as the hole-transport layer and the electron blocking layer, respectively; and 1,3,5-tris(*N*-phenylbenzimidazole-2-yl)benzene (TPBi) was used as the electron-transport layer. The molecular structure of organic materials involved in OLED fabrication and the device structure and energy level diagrams are shown in Scheme 1.

Fig. 8 reveals the EL spectra, current density–voltage-luminance (*J*–*V*–*L*), current efficiency–current density–power efficiency (CE–*J*–PE), and the external quantum efficiency–luminance (EQE–*L*) characteristic curves of **TPA-AN-NA** and **TPA-AN-TFP**-based non-doped devices, where the key performance parameters are also listed in Table 2. Two non-doped devices all realize blue emission with peaks located at 464 nm and 472 nm and corresponding to the CIE coordinates of (0.14, 0.16) and (0.15, 0.24) for **TPA-AN-NA** and **TPA-AN-TFP**-based devices, respectively.

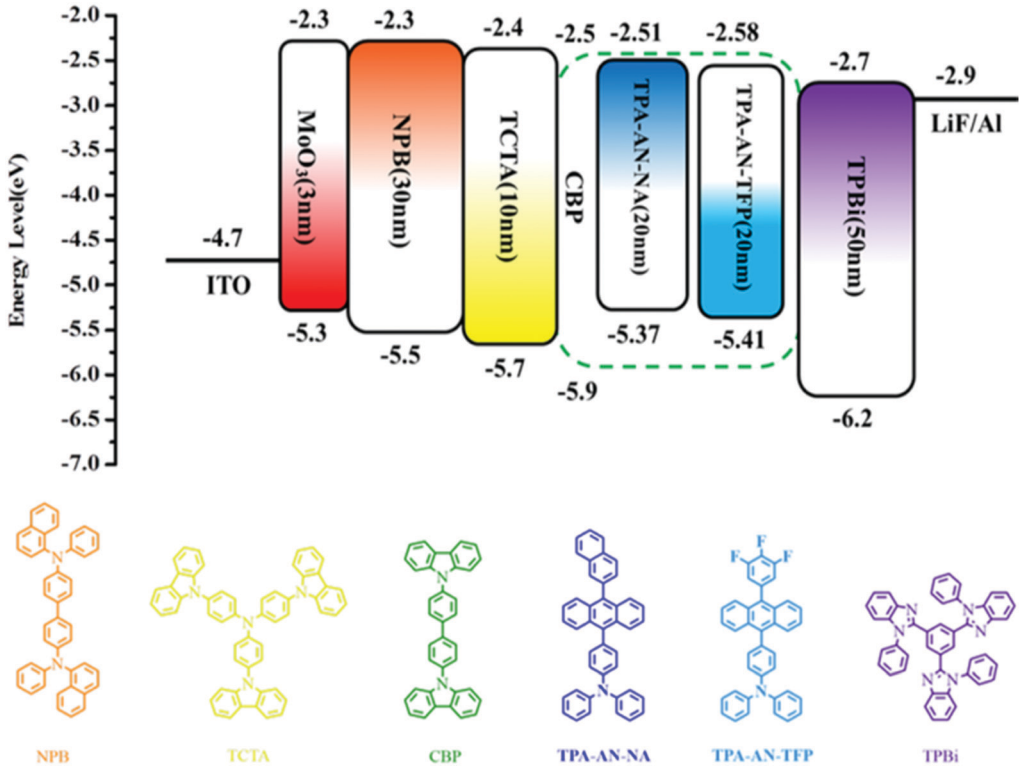

Scheme 1 Energy-level diagram and molecular structures of all materials used in devices.

Clearly, their EL spectra are similar to their PL spectra in thin films, indicating that the EL emissions originate from the two emitting materials themselves. The EL spectra for the two devices show no changes at various voltages from 4 to 9 V, as shown in Fig. S8 and S9 (ESI†), exhibiting extremely high stability. As shown in Fig. 8(b), the **TPA-AN-NA**-based device shows a low turn-on voltage of 3.0 V, which is lower than that for the **TPA-AN-TFP**-based devices, which can be ascribed to a smaller energy barrier between **TPA-AN-NA** and functional layers. And the two devices achieve a high luminance of 8344 and 9899 cd m^{-2} for **TPA-AN-NA** and **TPA-AN-TFP**-based devices, respectively. In addition, the two devices also achieve an excellent device efficiency with the maximum CE, PE, and EQE of 6.37 cd A^{-1}, 6.68 lm W^{-1}, and 4.93% for the **TPA-AN-NA**-based device and 4.91 cd A^{-1}, 3.33 lm W^{-1}, and 2.77% for the **TPA-AN-TFP**-based device. The higher efficiency of the **TPA-AN-NA**-based device is owing to the higher fluorescence quantum yield than that of **TPA-AN-TFP**-based in the film state.

Considering the influence of the aggregation effect on the emitters, both **TPA-AN-NA** and **TPA-AN-TFP** are doped in 4,4′-bis(*N*-carbazolyl)-1,1′-biphenyl (CBP) to fabricate two doped devices with the structure of ITO/MoO_3 (3 nm)/NPB (30 nm)/TCTA (10 nm)/CBP: 20 wt% **TPA-AN-NA** or **TPA-AN-TFP** (20 nm)/TPBi (50 nm)/LiF (1 nm)/Al (100 nm). As seen in Fig. 8(a), similar to the non-doped devices, the doped devices also realize good blue emission with peaks at 460 and 468 nm. But the doped devices achieve higher EL performance, for example, the maximum luminance, CE, PE, and EQE are up to 8246 cd m^{-2}, 7.16 cd A^{-1}, 6.09 lm W^{-1}, and 5.44% for the **TPA-AN-NA**-based doped device and 11450 cd m^{-2}, 5.17 cd A^{-1}, 4.16 lm W^{-1}, and 3.38% for the **TPA-AN-TFP**-based doped device, respectively. For higher device performance, it is likely attributed to a reduced exciton quenching in doped devices. The radiative exciton utilization (η_r) for all devices can be calculated using eqn (3)

$$\mathrm{EQE} = \gamma \times \Phi_{\mathrm{PL}} \times \eta_r \times \eta_{\mathrm{out}} \quad (3)$$

where γ is the carrier recombination efficiency, which is assumed to be 100%; Φ_{PL} is the PL quantum yield of emitters.[33] The Φ_{PL}s of **TPA-AN-NA** and **TPA-AN-TFP** in non-doped films were measured to be 30.68 and 23.96%, and 48.07 and 34.72% when doped in CBP films, respectively; η_r is the radiative exciton yield and η_{out} is the light out-coupling efficiency, which is generally considered to be 20%. The calculated η_r values of **TPA-AN-NA** and **TPA-AN-TFP**-based non-doped devices are 80.35 and 57.80% respectively, while the η_r values of the doped devices are 56.58 and 48.68%. These values of radiative exciton yields have broken the limitation of 25% for fluorescent OLEDs, indicating that there was an effective up-conversion process from some triplet excitons to singlet ones in these devices.

Generally, a high η_r and RISC in fluorescent devices can be achieved by three mechanisms: thermally activated delayed fluorescence (TADF),[34] triplet–triplet annihilation (TTA),[35] and the formation of an HLCT excited state. The transient PL spectra of **TPA-AN-NA** in the film and THF solution show only the single exponential decay with lifetimes of 3.42 and 2.31 ns, respectively (Fig. S6 and Table S1, ESI†). For **TPA-AN-TFP**, the lifetimes in THF solution and the film are 5.20 and 2.12 ns (Table S2, ESI†), respectively. No delayed lifetimes in the range of μs were observed.

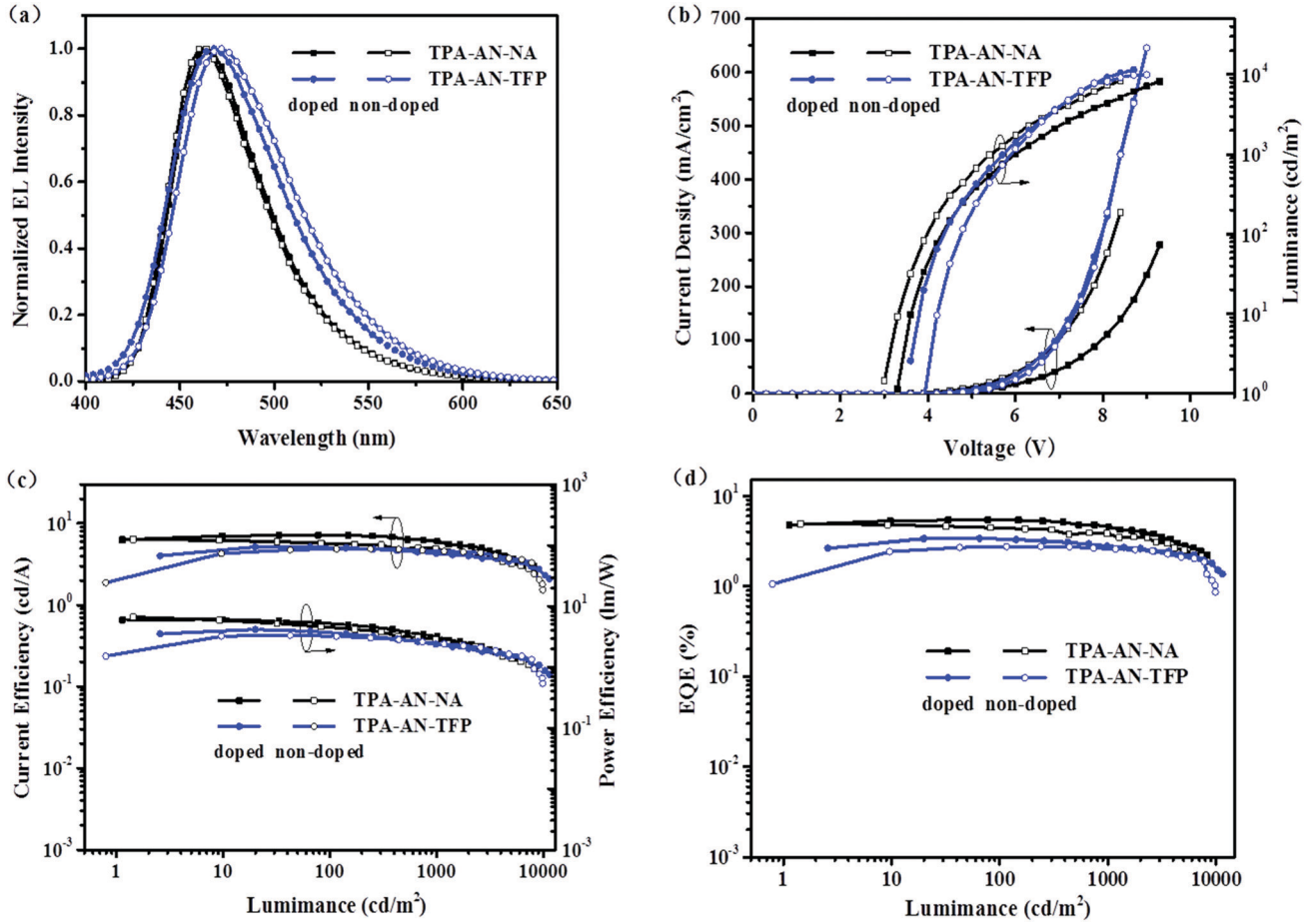

Fig. 8 (a) EL spectra at a driven voltage of 8 V; (b) the *J*–*V*–*L* curve; (c) the CE–*L*–PE curve and (d) the EQE–*L* curve for non-doped and doped blue devices based on **TPA-AN-NA** and **TPA-AN-TFP**.

Table 2 EL performance of devices based **TPA-AN-NA** and **TPA-AN-TFP**

Emitter	λ_{max} (nm)	V_{on}[a] (V)	L_{max} (cd m^{-2})	CE_{max} (cd A^{-1})	PE_{max} (lm W^{-1})	EQE_{max} (%)	CIE (x, y)
TPA-AN-NA	464	3.0	8344	6.37	6.68	4.93	(0.14, 0.16)
CBP:**TPA-AN-NA**	460	3.3	8246	7.16	6.09	5.44	(0.14, 0.16)
TPA-AN-TFP	472	3.9	9899	4.91	3.33	2.77	(0.15, 0.24)
CBP:**TPA-AN-TFP**	468	3.6	11 450	5.17	4.16	3.38	(0.14, 0.20)

[a] Turn-on voltage estimated at a brightness of 1 cd m^{-2}.

Furthermore, the correlations between the luminance and the current density of all devices were linear[36,37] (Fig. S10, ESI†). These results indicate that the high η_r values do not result from TADF or TTA processes. Hence, the HLCT excited states are mainly responsible for the high radiative utilization from triplets.

Conclusions

In this work, two novel blue fluorescent materials **TPA-AN-NA** and **TPA-AN-TFP** were designed and synthesized by linking a donor of triphenylamine (TPA) and both acceptors of anthracene derivatives. Both synthesized compounds show a hybrid local-excited and charge-transfer state. The resulting OLEDs with **TPA-AN-NA** and **TPA-AN-TFP** as emitters exhibit blue emission with electroluminescence peaks at 464 and 472 nm and with the CIE coordinates of (0.14, 0.16) and (0.15, 0.24), respectively. In addition, the **TPA-AN-NA**-based blue device achieves high external quantum efficiency exceeding the theoretical limit of 5% in fluorescent blue OLEDs, reaching 5.44%. The achievement of high singlet exciton-utilizing efficiencies of 80.35 and 56.58% is due to the formation of the HLCT excited states.

Experimental section

Materials and methods

All the reagents and solvents used for the syntheses and measurements were purchased from commercial suppliers and were used without further purification unless otherwise noted.

^{1}H NMR and ^{13}C NMR spectra were measured with a Switzerland Bruker DR × 600 spectrometer. UV-vis absorption spectra were measured using a Lambda Bio 40 spectrometer. Photoluminescence (PL) spectra were recorded using a HORIBA FluoroMax-4 spectrophotometer. Absolute quantum yields were determined through an absolute method employing an integrating sphere. Thermogravimetric analysis (TGA) curves were measured using a Netzsch TG 209F3 thermal analyser under a dry nitrogen atmosphere heating from room temperature up to 800 °C at a rate of 10 °C min^{-1}. Differential scanning calorimetry (DSC) was performed using a DSC Q2000 calorimeter at a heating rate of 10 °C min^{-1} from 40 to 300 °C, and then cooling down to room temperature rapidly, and heating up to 300 °C at a heating rate of 10 °C min^{-1} again; the melting temperature (T_m) was obtained from the first heating scan and the glass transition temperature (T_g) was determined from the second heating scan. Cyclic voltammetry (CV) was carried out in a solution of tetrabutylammonium perchlorate (0.1 M) in acetonitrile at a scan rate of 100 mV s^{-1} at room temperature using a conventional three electrode cell, which consisted of a working electrode platinum plate, a counter electrode platinum wire, and a reference calomel electrode.

DFT calculation

Theoretical calculations were performed using the Gaussian 03 package. Geometry optimization was performed by density functional theory (DFT) with B3LYP/6-31G(d) basis sets.

OLED fabrication and characterization

OLEDs with an area of 3 × 3 mm^2 were fabricated by vacuum deposition onto indium tin oxide (ITO) glass substrates. The substrates were cleaned, in the following order, with deionized water, acetone, and ethanol. The electroluminescence (EL) spectra and CIE coordinates were measured using a PR-655 spectrophotometer. The current density–voltage–luminance (*J–V–L*) characteristics of the OLEDs were recorded using Keithley 2400 Source Meter and ST-900M Spot Brightness Meter instruments.

Synthesis of TPA-AN-NA and TPA-AN-TFP

Synthesis of 4-(10-(naphthalen-2-yl)anthracen-9-yl)-*N*,*N*-diphenylaniline (TPA-AN-NA). A mixture of 4-bromo-*N*,*N*-diphenylaniline (0.973 g, 3 mmol), 9,9-diphenyl-9,10-(10-(naphthalen-2-yl)anthracen-9-yl)boronic acid (1.15 g, 3.3 mmol), $Pd(PPh_3)_4$ (0.173 g, 0.15 mmol) and K_2CO_3 (2.0 M aqueous solution, 10.0 mL) were dissolved in 30 mL 1,2-dimethoxyethane, and then heated to reflux for 12 h. After cooling to room temperature, the solution was extracted with dichloromethane. The organic material was dried using anhydrous $MgSO_4$ and concentrated. Then the crude product was purified by silica gel chromatography. The desired product was obtained as yellow powder (1 g, yield: 63%). Purity can be reached 96%. ^{1}H NMR (600 MHz, DMSO, δ): 8.19 (d, J = 8.7 Hz, 1H), 8.12 (d, J = 7.8 Hz, 1H), 8.05–8.01 (m, 2H), 7.77 (dd, J = 5.4, 4.3 Hz, 2H), 7.67–7.59 (m, 5H), 7.48 (td, J = 8.8, 6.4, 1.3 Hz, 2H), 7.43–7.38 (m, 8H), 7.25–7.22 (m, 6H), and 7.13 (td, J = 7.4, 1.1 Hz, 2H). ^{13}C NMR (151 MHz, $CDCl_3$, δ): 146.01, 145.38, 135.32, 134.88, 131.62, 130.89, 130.32, 128.36, 127.76, 127.56, 126.26, 126.08, 125.24, 124.57, 124.36, 123.20, 122.88, and 121.40.

Synthesis of *N*,*N*-diphenyl-4-(10-(3,4,5-trifluorophenyl)anthracen-9-yl)aniline (TPA-AN-TFP). 9-Bromo-10-(3,4,5-trifluorophenyl)-anthracene (**1**) and *N*,*N*-diphenyl-4-(10-(3,4,5-trifluorophenyl)-anthracen-9-yl)aniline (**TPA-AN-TFP**) were prepared with a similar procedure to that of **TPA-AN-NA**. The desired product was obtained as yellow-green powder (0.6 g, yield: 60%). Purity was 98%. ^{1}H NMR (600 MHz, $CDCl_3$, δ): 7.88–7.84 (m, 2H), 7.64–7.59 (m, 2H), 7.42–7.39 (m, 4H), 7.34 (t, J = 7.9 Hz, 4H), 7.30–7.25 (m, 8H), and 7.10 (dt, J = 18.2, 7.1 Hz, 4H). ^{13}C NMR (151 MHz, $CDCl_3$, δ): 150.68, 150.31, 141.23, 136.01, 134.93, 132.94, 132.59, 132.33, 130.28, 128.78, 128.06, 127.71, 126.14, 125.87, and 118.58.

Conflicts of interest

There are no conflicts to declare.

Acknowledgements

Ames Laboratory is operated by Iowa State University for the US Department of Energy (USDOE) under Contract No. DE-AC 02-07CH11358. This work was financially supported by the National Natural Science Foundation of China (61705156, 21071108, 60976018, 61605138 and 61775155) and the Shanxi Provincial Key Innovative Research Team in Science and Technology (201513002-10). JS was partially supported by Basic Energy Sciences, Materials Science and Engineering Division, USDOE. We also thank professor Runfeng Chen of Nanjing University of Posts and Telecommunications for calculation data.

References

1 C. W. Tang and S. A. VanSlyke, *Appl. Phys. Lett.*, 1987, **51**, 913–915.
2 P. Tao, Y. Miao, Y. Zhang, K. Wang, H. Li, L. Li, X. Li, T. Yang, Q. Zhao, H. Wang, S. Liu, X. Zhou, B. Xu and W. Huang, *Org. Electron.*, 2017, **45**, 293–301.
3 J.-H. Jou, S. Kumar, A. Agrawal, T.-H. Li and S. Sahoo, *J. Mater. Chem. C*, 2015, **3**, 2974–3002.
4 P. Tao, Y. Zhang, J. Wang, L. Wei, H. Li, X. Li, Q. Zhao, X. Zhang, S. Liu, H. Wang and W. Huang, *J. Mater. Chem. C*, 2017, **5**, 9306–9314.
5 S. Wang, M. Qiao, Z. Ye, D. Dou, M. Chen, Y. Peng, Y. Shi, X. Yang, L. Cui, J. Li, C. Li, B. Wei and W.-Y. Wong, *iScience*, 2018, **9**, 532–541.
6 Y. Feng, P. Li, X. Zhuang, K. Ye, T. Peng, Y. Liu and Y. Wang, *Chem. Commun.*, 2015, **51**, 12544–12547.
7 K. S. Yook and J. Y. Lee, *Adv. Mater.*, 2012, **24**, 3169–3190.
8 J. R. Sheats, H. Antoniadis, M. Hueschen, W. Leonard, J. Miller, R. Moon, D. Roitman and A. Stocking, *Science*, 1996, **273**, 884–888.
9 M. A. Baldo, D. F. O'Brien, M. E. Thompson and S. R. Forrest, *Phys. Rev. B: Condens. Matter Mater. Phys.*, 1999, **60**, 14422–14428.

10 Q. Zhang, J. Li, K. Shizu, S. Huang, S. Hirata, H. Miyazaki and C. Adachi, *J. Am. Chem. Soc.*, 2012, **134**, 14706–14709.
11 S. Chen, J. Lian, W. Wang, Y. Jiang, X. Wang, S. Chen, P. Zeng and Z. Peng, *J. Mater. Chem. C*, 2018, **6**, 9363–9373.
12 C.-L. Ho and W.-Y. Wong, *New J. Chem.*, 2013, **37**, 1665–1683.
13 S. Zhang, W. Li, L. Yao, Y. Pan, F. Shen, R. Xiao, B. Yang and Y. Ma, *Chem. Commun.*, 2013, **49**, 11302–11304.
14 W. Li, Y. Pan, R. Xiao, Q. Peng, S. Zhang, D. Ma, F. Li, F. Shen, Y. Wang, B. Yang and Y. Ma, *Adv. Funct. Mater.*, 2014, **24**, 1609–1614.
15 L. Yao, S. Zhang, R. Wang, W. Li, F. Shen, B. Yang and Y. Ma, *Angew. Chem., Int. Ed.*, 2014, **53**, 2119–2123.
16 X. Liang, Z. Wang, L. Wang, M. Hanif, D. Hu, S. Su, Z. Xie, G. Yu, Y. Bing and Y. Ma, *Chin. J. Chem.*, 2017, **35**, 1559–1568.
17 Y. Yu, L. Ma, X. Yang, H. Zhou, H. Qin, J. Song, G. Zhou, D. Wang and Z. Wu, *Adv. Opt. Mater.*, 2018, **6**, 1800060.
18 B. Liu, Z.-W. Yu, D. He, Z.-L. Zhu, J. Zheng, Y.-D. Yu, W.-F. Xie, Q.-X. Tong and C.-S. Lee, *J. Mater. Chem. C*, 2017, **5**, 5402–5410.
19 J. Shi, L. Xu, C. Chen, X. Lv, Q. Ding, W. Li, S. Xue and W. Yang, *Dyes Pigm.*, 2019, **160**, 962–970.
20 S. Liu, X. Zhang, C. Ou, S. Wang, X. Yang, X. Zhou, B. Mi, D. Cao and Z. Gao, *ACS Appl. Mater. Interfaces*, 2017, **9**, 26242–26251.
21 J. Jiang, D. Hu, M. Hanif, X. Li, S. Su, Z. Xie, L. Liu, S. Zhang, B. Yang and Y. Ma, *Adv. Opt. Mater.*, 2016, **4**, 2109–2118.
22 Y. Zhi, B. Zhao, R. Cao, Y. Xu, J. Wang, D. Dang, C. Gao and L. Meng, *Dyes Pigm.*, 2018, **153**, 291–299.
23 H. Yu, H. Liu, H. Tan, H. Yao, Y. Song, S. Zhu, N. Song, B. Zhang and S. Guan, *Dyes Pigm.*, 2018, **158**, 97–103.
24 R. Braveenth, I.-J. Bae, Y. Wang, S. Kim, M. Kim and K. Chai, *Appl. Sci.*, 2018, **8**, 1168.
25 A. M. Thangthong, D. Meunmart, N. Prachumrak, S. Jungsuttiwong, T. Keawin, T. Sudyoadsuk and V. Promarak, *Tetrahedron*, 2012, **68**, 1853–1861.
26 J. Huang, J. H. Su, X. Li, M. K. Lam, K. M. Fung, H. H. Fan, K. W. Cheah, C. H. Chen and H. Tian, *J. Mater. Chem.*, 2011, **21**, 2957–2964.
27 Z.-Y. Xia, Z.-Y. Zhang, J.-H. Su, Q. Zhang, K.-M. Fung, M.-K. Lam, K.-F. Li, W.-Y. Wong, K.-W. Cheah, H. Tian and C. H. Chen, *J. Mater. Chem.*, 2010, **20**, 3768–3774.
28 L. Wang, Z.-Y. Wu, W.-Y. Wong, K.-W. Cheah, H. Huang and C. H. Chen, *Org. Electron.*, 2011, **12**, 595–601.
29 D. Zhang, X. Song, H. Li, M. Cai, Z. Bin, T. Huang and L. Duan, *Adv. Mater.*, 2018, **30**, 1707590.
30 Z. R. Grabowski, R. Krystyna and R. Wolfgang, *J. Cheminf.*, 2003, **34**, 3899–4032.
31 Q. Wan, B. Zhang, J. Tong, Y. Li, H. Wu, H. Zhang, Z. Wang, Y. Pan and B. Z. Tang, *Phys. Chem. Chem. Phys.*, 2019, **21**, 9837–9844.
32 W. Li, D. Liu, F. Shen, D. Ma, Z. Wang, T. Feng, Y. Xu, B. Yang and Y. Ma, *Adv. Funct. Mater.*, 2012, **22**, 2797–2803.
33 S. Zhang, L. Yao, Q. Peng, W. Li, Y. Pan, R. Xiao, Y. Gao, C. Gu, Z. Wang, P. Lu, F. Li, S. Su, B. Yang and Y. Ma, *Adv. Funct. Mater.*, 2015, **25**, 1755–1762.
34 H. Uoyama, K. Goushi, K. Shizu, H. Nomura and C. Adachi, *Nature*, 2012, **492**, 234–238.
35 D. Chen, G. Xie, X. Cai, M. Liu, Y. Cao and S. J. Su, *Adv. Mater.*, 2016, **28**, 239–244.
36 P. Y. Chou, H. H. Chou, Y. H. Chen, T. H. Su, C. Y. Liao, H. W. Lin, W. C. Lin, H. Y. Yen, I. C. Chen and C. H. Cheng, *Chem. Commun.*, 2014, **50**, 6869–6871.
37 C. Ganzorig and M. Fujihira, *Appl. Phys. Lett.*, 2002, **81**, 3137–3139.

